Growth and Transformation of TiO_2 Crystallites in Aerosol Reactor

Atsuo Kobata, Katsuki Kusakabe, and Shigeharu Morooka
Dept. of Applied Chemistry, Kyushu University, Fukuoka 812, Japan

Rate processes concerning the formation of TiO_2 fine crystalline particles by the gas-phase reaction of $TiCl_4$ and O_2 are studied using aerosol reactors. Chemical reaction of $TiCl_4$, sintering of particles, mixing of reactants, and transformation from anatase to rutile are evaluated as the system parameters of the simulation model proposed. The crystallite size in the range of 55–65 nm at 1,273 K is predicted well by a model that assumes the maximum fusible particle size, 15 nm in this case.

The defect concentration in the TiO_2 crystallites strongly affects the transformation rate, and anatase particles produced at 1,173 K are transformed to rutile more rapidly than those produced at 1,373 K. The transformation is simulated quantitatively by the model with the coordinates for elapsed time, particle size and rutile fraction. The model can be applied to such particle production processes as collision, sintering and crystal transformation occurring simultaneously.

Introduction

Titanium oxide having a high refractive index and good coloring property is useful as a pigment, and is important as an electronic material and catalyst support. Crystalline TiO_2 particles produced industrially are in the crystal form of anatase or rutile. Figure 1 shows the general scheme for the formation of TiO_2 crystallites by the following gas-phase reaction.

$$TiCl_4 + O_2 \rightarrow TiO_2 + 2Cl_2 \qquad (1)$$

TiO_2 monomer generated by reaction 1 forms metastable anatase clusters by homogeneous nucleation. Then, the clusters grow by the heterogeneous condensation of TiO_2 vapor and by the coagulation-fusion mechanism. Some of them become anatase particles, and others are transformed into rutile particles that are thermochemically-stable.

Ulrich (1971) derived the particle concentration from the Brownian coagulation, assuming the instantaneous fusion of particles. George et al. (1973) produced TiO_2 particles by introducing $TiCl_4$ vapor to a CO-burning flame at temperatures up to 1,673 K. The average size of particle obtained was 20–60 nm, which agreed with the prediction of Ulrich (1971). In the experiment of Okuyama et al. (1986), ultrafine particles of TiO_2, SiO_2 and Al_2O_3 were produced by the thermal decomposition of alkoxide compounds. Particle size was qualitatively expressed by a model, in which clusters were divided into discrete sections while particles were expressed by a continuous size distribution function. Wu and Flagan (1988) proposed a population model assuming the discrete regime for clusters and the sectional regime for particles. These studies were carried out under the condition that the sintering of particles occurred instantaneously.

However, TiO_2 crystallites produced by the oxidation of $TiCl_4$ were much smaller than those predicted by the model of Ulrich (1971) (Morooka et al., 1989). This result indicates that the fusion rate of particles is not always instantaneous. The growth of aggregates caused by simple assemblage of primary particles (Ulrich and Riehl, 1982) is not discussed in this article, and "particle" means discrete crystallite hereafter.

Suyama et al. (1975) produced TiO_2 particles of 50–200 nm in size by the gas-phase reaction of the $TiCl_4$-O_2 system. Their result suggested that the nucleation of the rutile phase took place predominantly at the latter stage, where the monomer concentration was low. The rutile content was on the order of $(TiCl_4\text{-}O_2) < (TiCl_4\text{-}H_2O) < (TiCl_4\text{-}H_2O\text{-}H_2) < (TiCl_4\text{-}H_2\text{-}CO_2)$ (Kato and Suyama, 1974), which means that the production of rutile TiO_2 is facilitated by the introduction of crystal deficiencies. This result may be related to the experiments of Matsumoto et al. (1967) who produced TiO_2 particles by the

Correspondence concerning to this article should be addressed to S. Morooka.

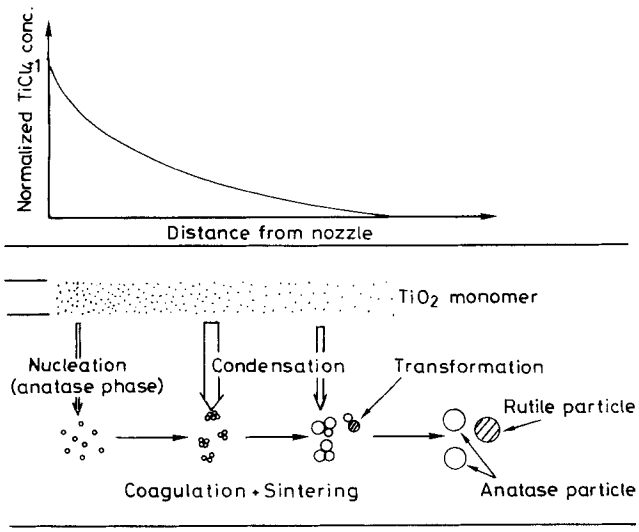

Figure 1. Formation of TiO_2 particles.

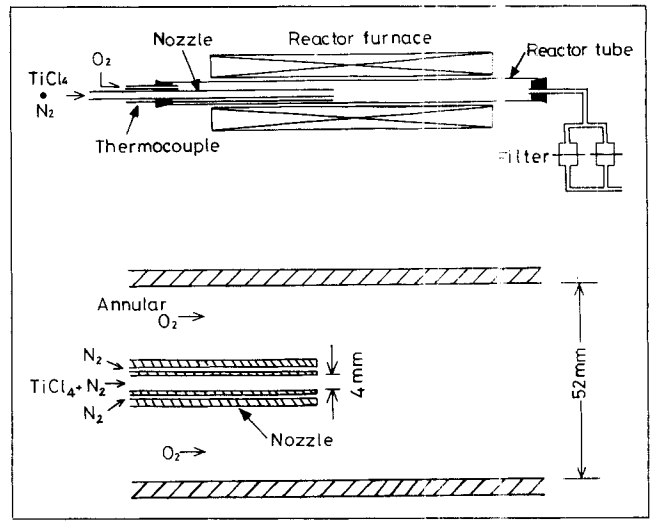

Figure 2. Experimental apparatus for generating ultrafine TiO_2.

gas-phase oxidation of $TiCl_4$ with air. When $TiCl_4$ and air were mixed at 298 K, particles obtained were about 1 μm in size and were mostly anatase. On the other hand, when $TiCl_4$ and air were mixed at a reaction temperature, rutile particles of 100–200 nm were generated, but no quantitative discussion was given.

In brief, no population models in the literature consider the sintering rate of particles and the transformation rate of crystal structure at the same time. To control the particle size and rutile content, we must establish a population model including these rate processes.

In this work, TiO_2 ultrafine particles are produced by the reaction of $TiCl_4$ and O_2. To simulate the total formation process of TiO_2 crystallites, the reaction rate of $TiCl_4$, collision rate of particles, fusion of particles, transformation rate from anatase to rutile, and mixing time of reactants in the reactor are all investigated quantitatively. A population model accounting for these factors is derived and solved numerically. The application of this model, however, is not limited to the TiO_2 production, which is adopted to demonstrate formation mechanism of fine particles.

Generation of TiO_2 Particles

Experimental setup

The formation of TiO_2 particles was carried out in a laminar-flow aerosol reactor, made of a 30- or 52-mm-ID mullite tube heated externally with a kanthal wire or a SiC resistance heater. The reactor was set horizontally or vertically, and the length of the effective reaction zone and flow rates were varied as indicated in Table 1. Figure 2 shows details of the nozzle in the reactor of system A. The inner nozzle was a 4-mm-ID and 6-mm-OD alumina tube, which was sheathed concentrically with an 8-mm-ID and 12-mm-OD alumina tube and was fixed on the center axis of the reactor. The sheath tube was not used in systems B, C, E, F, G, H, and I.

Reagent-grade $TiCl_4$ was put in a glass bottle that was placed in a constant-temperature bath. Then, $TiCl_4$ vapor was vaporized into nitrogen carrier gas, which had been dried by passing through a silica gel bed and an ethanol-dry ice trap, and introduced through the nozzle. The nitrogen was also sent through the sheath space to avoid solid deposition on the mouth of the nozzle. Oxygen, dried and diluted with nitrogen, was introduced into the reactor through the annular space. The reaction was carried out at temperatures above 1,123 K where the $TiCl_4$ conversion was 100%. Other conditions are listed in Table 2.

TiO_2 particles were collected on filter paper at the reactor exit. The average particle size was measured by X-ray diffraction for CuKα radiation using the silicon crystal internal standard. Particles were also characterized by transmission

Table 1. Reactor Dimensions and Gas Flow Rates*

Case	Key	Reactor	d_t mm	d_n mm	L mm	$Q_n(N_2+O_2)$ $cm^3 \cdot s^{-1}$	$Q_a(N_2+TiCl_4)$ $cm^3 \cdot s^{-1}$	Q_s $cm^3 \cdot s^{-1}$
A	○	vertical	52	4	150	25	6.7	13.3
B	⊙	vertical	52	4	150	25	3.3	—
C	⊖	vertical	52	9	150	6.7–25	3.3	—
D	△	horizontal	52	6	180	25	6.7	13.3
E	□	horizontal	52	4	180	10	3.3	—
F	◫	horizontal	30	4	80	10	3.3	—
G	■	horizontal	30	4	100	10	3.3	—
H+	▲	horizontal	28	4	50	**	**	—
I++	▼	horizontal	38	**	200	**	**	—

*Measured at atmospheric temperature and pressure
**Not given by authors
+Suyama et al. (1975)
++Matsumoto et al. (1967)

Table 2. Ranges of Experimental Conditions

Reaction temperature	1,123–1,473 K
Nozzle gas velocity*	1–1.3 $m \cdot s^{-1}$
Sheath gas velocity*	1–1.3 $m \cdot s^{-1}$
Outer annular gas velocity*	0.05–0.07 $m \cdot s^{-1}$
O_2 partial pressure	10–100 kPa
$TiCl_4$ partial pressure	1–7 kPa
Residence time in reaction zone*	0.08–0.2 s

*At the reaction temperature.

electron microscopy. The rutile content in TiO_2 particles was determined from the relative X-ray diffraction intensity corresponding to anatase ⟨101⟩ and rutile ⟨110⟩ reflection.

$$M_A/M_R = K_c I_A/I_R \tag{2}$$

Then, the mass fraction of rutile becomes:

$$M_R/(M_A+M_R) = 1/(1+K_c I_A/I_R) \tag{3}$$

where K_c is given as 1.26 by Spurr and Myers (1957).

Particle size

Figure 3 shows the effect of initial oxygen concentration on TiO_2 particle size produced at 1,273 K. The particle size was in the range of 55–65 nm where the oxygen concentration fraction is higher than 0.4. In one case, the weight-mean size of particles was 58 nm from TEM pictures and 52 nm from the XRD. This coincidence indicates that the TiO_2 particles were mostly single crystals. When large and small particles were present simultaneously, the XRD gave an inaccurate value. Therefore, the weight-mean size from TEM pictures was adopted as the representative particle size. The effect of the reactor configuration shown in Table 1 was not evident. Typical crystallites size distributions were shown elsewhere (Morooka et al., 1989).

Rutile content

The effect of reaction temperature on the mass fraction of rutile in TiO_2 particles is shown in Figure 4. Rutile content reported by Suyama et al. (1975) and Matsumoto et al. (1967) are also plotted in the figure. The mass fraction of rutile increased with the increase in reaction temperature in the range of $T<1{,}273$ K and with the decrease in temperature above 1,273 K. Because the activation energy for transformation from anatase to rutile is of the order of 400 $kJ \cdot mol^{-1}$ (Mackenzie, 1975), the mass fraction of rutile is presumed to increase with increasing reaction temperature. A maximum rutile content, however, was observed clearly around 1,273 K. The data shown by the broken line were probably taken in an atmosphere contaminated by deficiency-forming materials.

Rate Processes Related to TiO_2 Formation

Reactivity of $TiCl_4$

Oxygen containing 3 vol. % $TiCl_4$ was introduced into the empty reactor of 30-mm-ID at a temperature of 723–973 K. Chlorine, produced by reaction 1, was absorbed into a KI solution. I_2 generated was determined by redox titration with

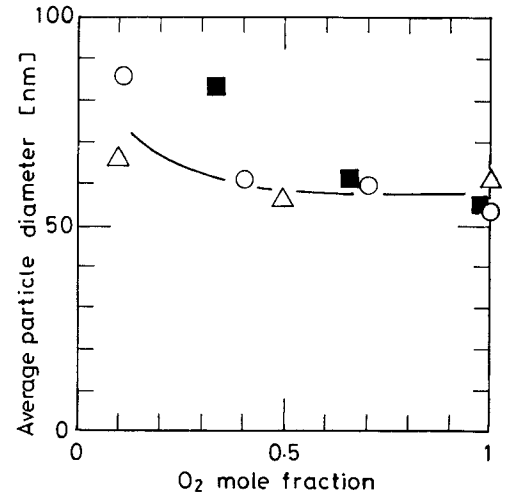

Figure 3. Effect of initial O_2 concentration on TiO_2 particle size.

a 0.01 $mol \cdot L^{-1}$ $Na_2S_2O_3$ solution, and the reaction rate of $TiCl_4$ with O_2 was obtained. The effective length of the heated zone was 7 cm, and the mean residence time in the reaction zone was controlled so that the conversion of $TiCl_4$ might be smaller than 0.5 in this experiment. Assuming that the reaction is first-order with respect to $TiCl_4$ in large excess of oxygen (Suyama and Kato, 1976; Toyama et al., 1990), the reaction rate is expressed by

$$dp_{TiCl_4}/dt = -k_{TO} p_{TiCl_4} \tag{4}$$

The temperature dependence of k_{TO} is shown in Figure 5. The results together with those in the literature are correlated by

$$k_{TO} = 2.5 \times 10^5 \exp[-102\ kJ \cdot mol^{-1}/(RT)] \tag{5}$$

where the unit of k_{TO} is s^{-1}. Pratsinis et al. (1990) also measured the reaction rate of $TiCl_4$ in the oxygen concentration range 0.2–9.2 kPa. The hatched zone in Figure 5 shows their data extraporated to the oxygen concentration 100 kPa.

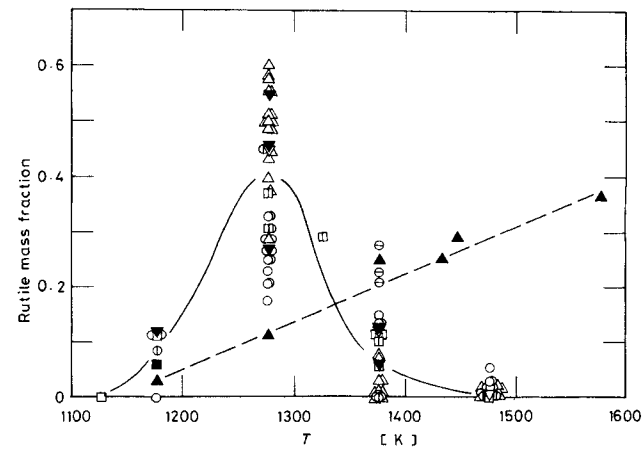

Figure 4. Reaction temperature vs. weight fraction of rutile in TiO_2 particles.

Keys are shown in Table 1.

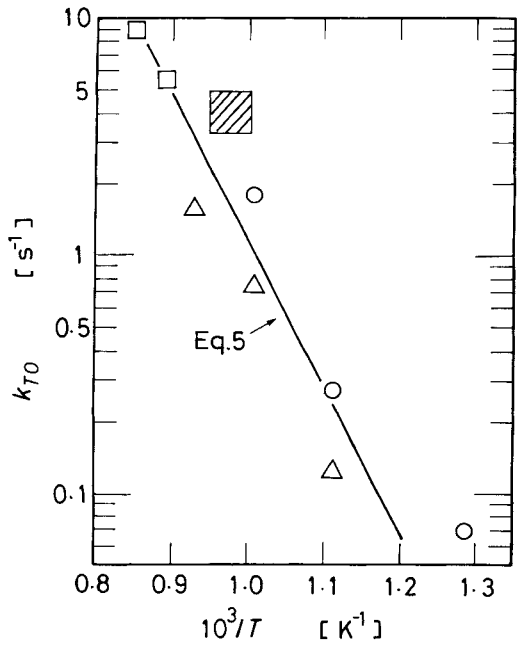

Figure 5. Temperature dependence of $TiCl_4$ reaction rate coefficient.

○, this work; △, Suyama et al. (1976); □, Toyama et al. (1990); hatched area, Pratsinis et al. (1990)

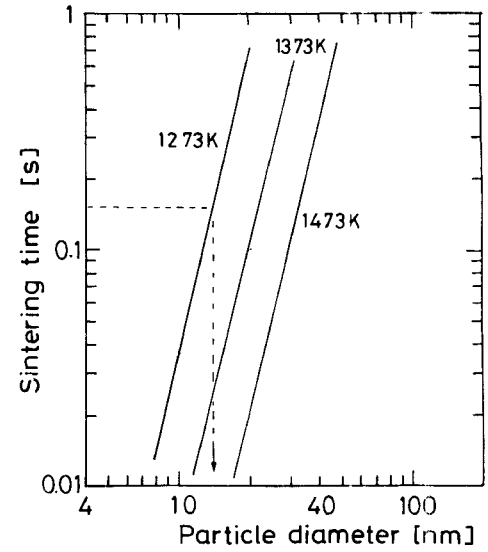

Figure 6. Time required for sintering of equal-sized TiO_2 spheres.

Sintering rate of TiO_2 particles

TiO_2 particles collide with one another due to Brownian motion and fuse into a new crystallite in a finite time. Sintering between equal-sized spheres proceeds through the neck growth and is evaluated by the grain boundary model. We calculated the time-dependent growth of the neck based on the model of Coblenz et al. (1980) without the initial sintering assumption. The result indicates that the curvature between the spheres disappears when the ratio of the neck length ℓ_n to the initial sphere radius r_I reaches about 0.83. This value is close to that for the surface diffusion model obtained by Nichols and Mullins (1965). If this point is considered as the completion of sintering, the dimensionless time period required for the sintering is given by

$$bD_b\gamma\Omega t/(k_BTr_I^4)=0.013 \tag{6}$$

where bD_b is the grain boundary diffusion coefficient. The correlation of bD_b by Astir and Vergnon (1976) gives larger values than that by Anderson (1967). Morooka et al. (1989) produced TiO_2 crystallites using the reactor F in Table 1 at 1,273 K with a complete conversion of $TiCl_4$ and introduced the aerosol continuously into a heating zone connected to the reactor in series. After the annealing for 1 s in the heating zone at 1,473 K, the particles grew from 55 nm to 130 nm. This result can be explained when the diffusion coefficient of Astir and Vergnon (1976) is used. The value of bD_b of Anderson (1967) is too small to explain this sintering. In the present analysis, therefore, we adopt the following correlation (Astir and Vergnon, 1976).

$$bD_b=1.6\times10^{-14}\exp[-258\ \text{kJ}\cdot\text{mol}^{-1}/(RT)] \tag{7}$$

where the unit of bD_b is $m^3\cdot s^{-1}$. By rearranging Eqs. 6 and 7, the sintering time is obtained.

$$t=1.4\times10^{21}r_I^4\exp[258\ \text{kJ}\cdot\text{mol}^{-1}/(RT)] \tag{8}$$

where t and r_I are in the units of s and m, respectively. Ω and γ are $1.57\times10^{-29}m^3$ and $0.6\ J\cdot m^{-2}$ (Anderson, 1967). Figure 6 shows the sintering time calculated from Eq. 8 in the range of 1,173-1,470 K. About 15 nm (r_I=7.5 nm) is the maximum size of TiO_2 particles that can be fused at 1,273 K within a residence time of 0.16 s, which is a typical condition of our experiments. As shown in Figure 3, however, the particles of 55-65 nm in diameter were actually obtained under the same condition. This discrepancy is caused by the growth through the heterogeneous deposition of TiO_2 vapor and the coagulation of smaller particles, as discussed later.

Transformation from anatase to rutile

TiO_2 particles of different origins were loosely placed in a platinum boat and quickly pushed into the furnace, which was kept at a prescribed temperature. After annealing for 1-90 min in an air flow, the boat was taken out of the furnace. The results show that the transformation rate depends strongly on the conditions, under which the particles were produced. The higher the defect concentration in the crystallites, the faster the transformation rate. Figure 7 shows time-dependent curves for the transformation of anatase particles produced at 1,173 K in this article. The result indicates that the transformation occurs more quickly at a higher annealing temperature.

The transformation is initiated by the formation of rutile nuclei on the surface of an anatase particle, followed by the linear growth of rutile phase toward the particle interior (Mackenzie, 1975). Once a rutile nucleus is formed on any part of the surface, the particle is assumed to be immediately covered by thin rutile phase. This is quite possible because surface diffusion is much faster than diffusion toward the interior.

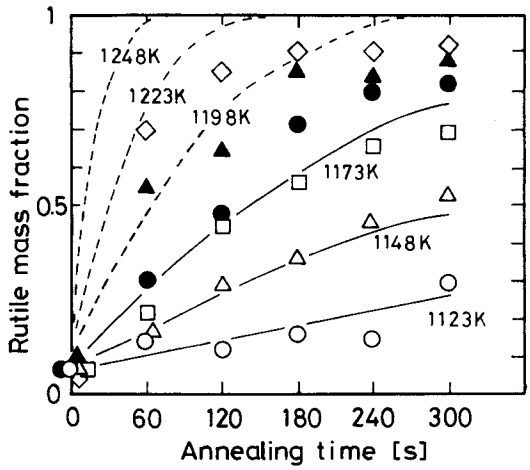

Figure 7. Time-dependent changes in transformation of particles produced at 1,173 K.

Annealing temperature: ○, 1,123 K; △, 1,148 K; □, 1,173 K; ●, 1,198 K; ▲, 1,223 K; ◇, 1,248 K. Lines are calculated from Eq. 13.

Here, the particles are spherical with the same size d_t, and the number-based fraction of particles covered by the rutile film is denoted by α_R. Then, the volume fraction of the rutile-covered particles is expressed as $(1/6)\pi d_t^3 \alpha_R$. If the evolution rate of rutile-covered particles is proportional to the surface area of anatase particles, we obtain:

$$\frac{d_t^3}{6}\frac{d\alpha_R}{dt} = d_t^2 k_N (1-\alpha_R) \tag{9}$$

Equation 9 is solved with the initial condition

$$t=0,\ \alpha_R = \alpha_{R0} \tag{10}$$

and we get

$$\ln[(1-\alpha_{R0})/(1-\alpha_R)] = (6k_N/d_t)t \tag{11}$$

Applying the unreacted-core model (Levenspiel, 1972) to the growth of the rutile phase in the anatase particle, the volume fraction of the rutile in the particle at time t, $f_R(t)$ is given by the following equation

$$[1-f_R(t)]^{1/3} = 1-(k_R/d_t)t \tag{12}$$

where k_R is the linear growth rate of the rutile phase moving into the anatase particle. When the density of anatase and rutile is assumed to be identical, the mass fraction of the rutile phase in particles of d_t after the annealing period t_0 is given by

$$M_R/(M_A+M_R) = \int_0^{t_0} (d\alpha_R/dt) f_R(t_0-t)\,dt \tag{13}$$

where $f_R(t_0-t)$ is unity if $1-(k_R/d_t)(t_0-t)$ is negative.

Figure 8 shows transmission electron micrographs (bright image) of particles produced at 1,173 K and those after annealing at 1,198 K for 1 min. When the annealing temperature was higher than 1,198 K, some crystallites were sintered as indicated in the lower picture. Therefore, the rutile transformation data in Figure 7 in the range of $T \leq 1{,}173$ K were used to calculate the transformation rate coefficients.

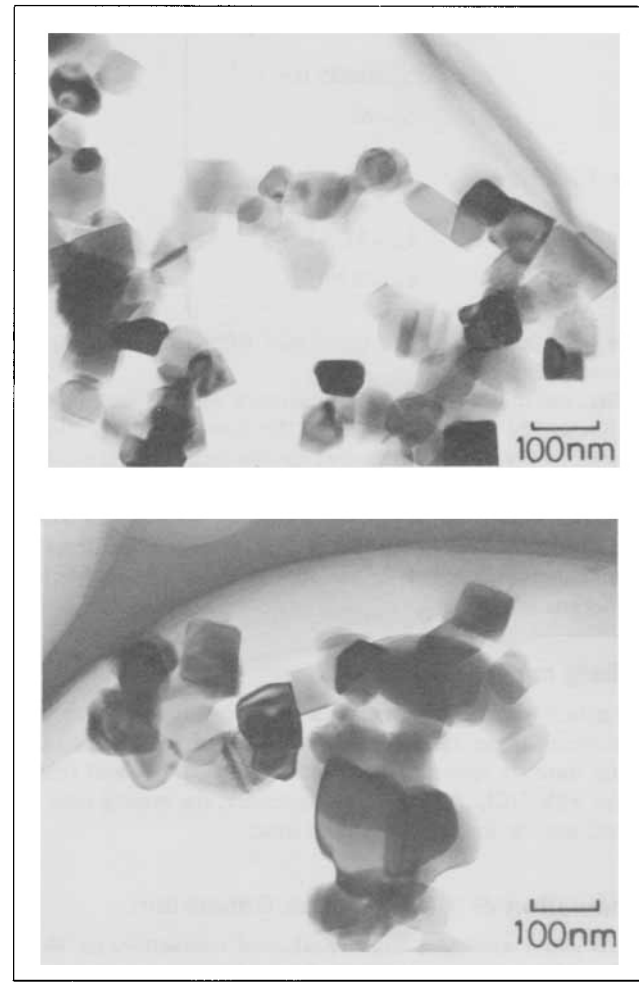

Figure 8. Transmission electron micrograph of TiO_2 particles.

Upper, particles produced at 1,173 K; lower, those after annealing at 1,198 K for 1 min

The linear growth rate of rutile for the particles produced at 1,173 K was very fast, and the rate-determining step was the nucleation of the rutile phase on the anatase surface. Then the value of k_N, a function of annealing temperature, was determined by the curve-fitting method in Figure 7.

$$k_N = 7.3\times 10^6 \exp[-389\ \text{kJ}\cdot\text{mol}/(\text{RT})] \tag{14}$$

where the unit of k_N is $\text{m}\cdot\text{s}^{-1}$. The TiO_2 particles generated at 1,373 K were also annealed at various temperatures. In this case, the transformation was affected by both k_N and k_R. Then, Eq. 14 was assumed to be applicable to the particles produced at 1,373 K, and the value of k_R was determined by the curve-fitting method. Thus, the transformation rate coefficients are obtained as follows:

For $T=1{,}173$ K,

$$k_N=0.035\ \text{nm}\cdot\text{s}^{-1}$$
$$k_R=\infty$$

For $T=1{,}373$ K,

$$k_N=11.5\ \text{nm}\cdot\text{s}^{-1}$$
$$k_R=0.17\ \text{nm}\cdot\text{s}^{-1} \qquad (15)$$

The lines in Figure 7 are calculated from Eq. 13, using the values of Eq. 15.

Because the defects in TiO_2 particles without additives are composed of oxygen vacancies, the defect concentration is related to the density measured by the pycnometric method. The particles produced at 1,173 K had a density of 3.69 $Mg\cdot m^{-3}$ and contained more defects than those produced at 1,373 K, the density of which was 3.8 $Mg\cdot m^{-3}$. The transformation from anatase to rutile is accelerated by the presence of defects (Mackenzie, 1975).

Mixing time of O_2 and $TiCl_4$

In the present experiments, the concentration of oxygen was 5-10 times higher than that of $TiCl_4$. Therefore, oxygen in the outer annular space diffused into the nozzle jet and reacted there with $TiCl_4$. As shown in Appendix, the mixing time was much shorter than the residence time.

Simulation of TiO_2 Particles Generation

To avoid solving a large number of unsteady-state simultaneous differential equations from monomer to i-mers, the discrete-sectional model derived from Gelbard et al. (1980) and Wu and Flagan (1988) is used in this work.

Figure 9 illustrates the size spectrum separated into two sections described by: 1. the number concentration of particles containing i monomers, N_i, starting from the monomer; and 2. the mass concentration, Q_ℓ, which is divided into sectioned classes with finite intervals. Assuming constant particle density, the particle size in the sectional regime is represented by the logarithm of the particle mass. In this article, the discrete regime extends from monomer to 9-mer, and the particle size in the sectional regime is divided into four sections per decade.

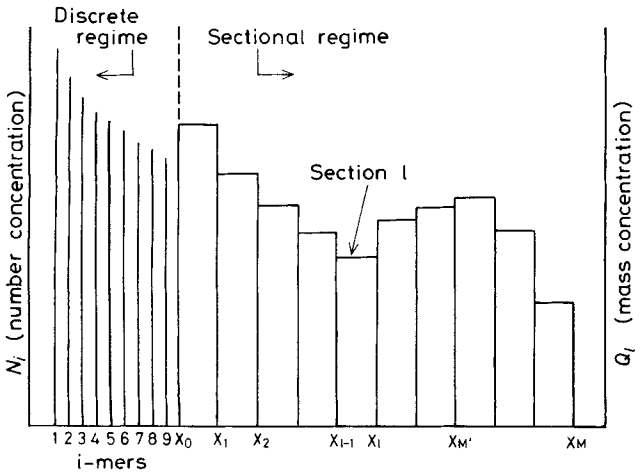

Figure 9. Aerosol size spectrum for discrete-sectional model.

The fundamental equations are the same as those of Wu and Flagan (1988) who assumed the instantaneous fusion of paired particles. As stated in the experimental results section, however, paired particles do not sinter during their residence in the reactor if the smaller particle belongs to the section larger than a given value M'. The evaporation and escape of monomers from clusters and particles can be neglected due to high supersaturation for the system of $TiCl_4$ and O_2. The monomer is generated at the rate expressed by Eqs. 4 and 5. Then the equations of mass balance are expressed by

$$\frac{dN_1}{dt}=-\sum_{i=1}^{9}\beta_{1i}N_1N_i-\sum_{r=1}^{M}{}^{1}\bar{\bar{\beta}}_{1r}Q_rN_1 \qquad (16)$$

$2\leqq i\leqq 9$:

$$\frac{dN_i}{dt}=\frac{1}{2}\sum_{j=1}^{i-1}\beta_{(i-j)j}N_{(i-j)}N_j-\sum_{j=1}^{9}\beta_{ij}N_iN_j-\sum_{r=1}^{M}{}^{1}\bar{\bar{\beta}}_{ir}Q_rN_i \qquad (17)$$

$1\leqq \ell\leqq M'$:

$$\frac{dQ_\ell}{dt}=\underbrace{\frac{1}{2}\sum_{i=1}^{\ell-1}\sum_{j=1}^{\ell-1}{}^{1}\bar{\beta}_{ij\ell}Q_iQ_j}_{①}-\underbrace{\sum_{i=1}^{\ell-1}{}^{2}\bar{\beta}_{i\ell}Q_iQ_\ell}_{②+③}-\underbrace{\frac{1}{2}{}^{3}\bar{\beta}_{\ell\ell}Q_\ell^2}_{④}$$

$$-\underbrace{\sum_{i=\ell+1}^{M}{}^{4}\bar{\beta}_{i\ell}Q_iQ_\ell}_{⑤}-\underbrace{\sum_{i=1}^{9}{}^{2}\bar{\bar{\beta}}_{i\ell}N_iQ_\ell}_{⑥}+\underbrace{\sum_{i=1}^{9}\sum_{r=1}^{\ell-1}{}^{3}\bar{\bar{\beta}}_{ir\ell}N_iQ_r}_{⑦}$$

$$+\underbrace{\frac{1}{2}\sum_{i=1}^{9}\sum_{j=1}^{9}{}^{4}\bar{\bar{\beta}}_{ij\ell}N_iN_j}_{⑧} \qquad (18)$$

$\ell>M'$:

$$\frac{dQ_\ell}{dt}=\underbrace{\frac{1}{2}\sum_{i=1}^{M'}\sum_{j=1}^{M'}{}^{1}\bar{\beta}_{ij\ell}Q_iQ_j+\sum_{i=1}^{M'}\sum_{j=M'+1}^{\ell-1}{}^{1}\bar{\beta}_{ij\ell}Q_iQ_j}_{①}-\underbrace{\sum_{i=1}^{M'}{}^{2}\bar{\beta}_{i\ell}Q_iQ_\ell}_{②+③}$$

$$-\underbrace{\sum_{i=1}^{9}{}^{2}\bar{\bar{\beta}}_{i\ell}N_iQ_\ell}_{⑥}+\underbrace{\sum_{i=1}^{9}\sum_{r=1}^{\ell-1}{}^{3}\bar{\bar{\beta}}_{ir\ell}N_iQ_r}_{⑦}+\underbrace{\frac{1}{2}\sum_{i=1}^{9}\sum_{j=1}^{9}{}^{4}\bar{\bar{\beta}}_{ij\ell}N_iN_j}_{⑧} \qquad (19)$$

The paths of ①, ②, ⑦, and ⑧ mean the mass entering section ℓ, while the paths of ③, ④, ⑤, and ⑥ are the

mass leaving section ℓ. ${}^1\bar{\beta}_{ij\ell}$, ${}^2\bar{\beta}_{i\ell}$, ${}^3\bar{\beta}_{\ell\ell}$, and ${}^4\bar{\beta}_{i\ell}$ are the inter- and intrasectional coagulation constants in the sectional regime, and ${}^1\bar{\bar{\beta}}_{ir}$, ${}^2\bar{\bar{\beta}}_{i\ell}$, ${}^3\bar{\bar{\beta}}_{ir\ell}$, and ${}^4\bar{\bar{\beta}}_{ij\ell}$ are the discrete-sectional coagulation coefficients. These coagulation coefficients are identical to those defined by Wu and Flagan (1988, Tables I and II of their paper). ${}^2\bar{\beta}_{i\ell}$ is composed of two paths ② and ③:

$$ {}^2\bar{\beta}_{i\ell} = {}^5\bar{\beta}_{i\ell} - {}^6\bar{\beta}_{i\ell} \tag{20} $$

$$ {}^5\bar{\beta}_{i\ell} = \int_{x_{i-1}}^{x_i}\int_{x_{\ell-1}}^{x_\ell} \frac{\theta[(u+v) \geqq v_\ell]\beta(u,v)}{v(x_i - x_{i-1})(x_\ell - x_{\ell-1})}\, dxdx \tag{21} $$

$$ {}^6\bar{\beta}_{i\ell} = \int_{x_{i-1}}^{x_i}\int_{x_{\ell-1}}^{x_\ell} \frac{\theta[(u+v) < v_\ell]\beta(u,v)}{u(x_i - x_{i-1})(x_\ell - x_{\ell-1})}\, dxdx \tag{22} $$

where x_ℓ is the logarithm of v_ℓ, which is the mass of a particle having the size of ℓ. $(x_\ell - x_{\ell-1})$ is the interval of the section ℓ on the logarithm scale. θ is a function that is unity when the inequality in the brackets is valid and is zero otherwise. The variables u and v are the mass of a particle in the ranges $(x_i - x_{i-1})$ and $(x_\ell - x_{\ell-1})$, respectively. The Brownian coagulation coefficient $\beta(u,v)$ is expressed by the interpolation formula applicable to spheres in the free molecule and continuum regime and is given by Fuchs (1964) and Wu and Flagan (1988). If $i > M'$ and $j > M'$, $\beta_{ij} = 0$. Using Eqs. 16-19, the weight-averaged size of TiO_2 crystallites,

$$ \sum_{\ell=1}^{M} Q_\ell d_\ell \Big/ \sum_{\ell=1}^{M} Q_\ell, $$

is calculated.

Figure 10 shows the effect of residence time in the reactor on the average particle size calculated by the above procedure at 1,273 K. The fusion of paired particles is assumed to stop when the smaller particle is larger than 10, 15, 20, 30 or 50 nm, which is expressed by M' in Eqs. 18 and 19. If we adopt 15 nm as the maximum sinterable size from Figure 6, the culated average particle size is about 50 nm for the residence time ~0.16 s and approximately agrees with the experimental results shown in Figure 3.

Simulation for Formation of Rutile Particles

Formation at 1,173 K

Figure 11 shows the mechanism of rutile transformation at the moment of coagulation for TiO_2 particles produced in the range of $T \leqq 1{,}273$ K. As indicated in the experimental results section, the rutile phase moves very quickly toward the inside of the particle once rutile nuclei are formed on the anatase surface at this temperature. The following cases are possible for the fusion of two particles.

Case 1: Fusion of Particles with the Same Crystal Form. The original crystal form is maintained.

Case 2: Fusion between Rutile and Anatase Particles. If the mass of the anatase particle is λ times larger than that of the rutile particle, the rutile mass is assumed to be incorporated into the abundant anatase mass and the fused new particle becomes anatase. In the other case, the merger of the rutile phase favors the transformation, and the newborn particle

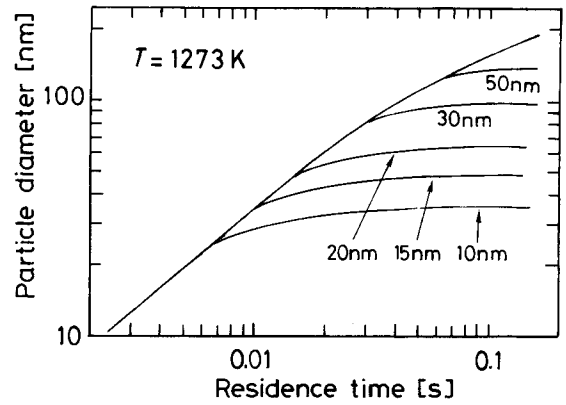

Figure 10. Effect of residence time in reactor on mean particle size.

becomes rutile. ${}^1W_{ij}$ means the rutile fraction in the new particle, which is formed by the fusion of an anatase particle of section i and a rutile particle of section j, and is expressed by the probability that the mass of a particle of section i is smaller than λ times that of section j.

$$ {}^1W_{ij} = \frac{\int_{x_{i-1}}^{x_i}\int_{x_{j-1}}^{x_j} \theta(u < \lambda v)(u+v)\, dxdx}{\int_{x_{i-1}}^{x_i}\int_{x_{j-1}}^{x_j} (u+v)\, dxdx} \tag{23} $$

and similarly

$$ {}^1W_{ji} = \frac{\int_{x_{j-1}}^{x_j}\int_{x_{i-1}}^{x_i} \theta(v < \lambda u)(u+v)\, dxdx}{\int_{x_{j-1}}^{x_j}\int_{x_{i-1}}^{x_i} (u+v)\, dxdx} \tag{24} $$

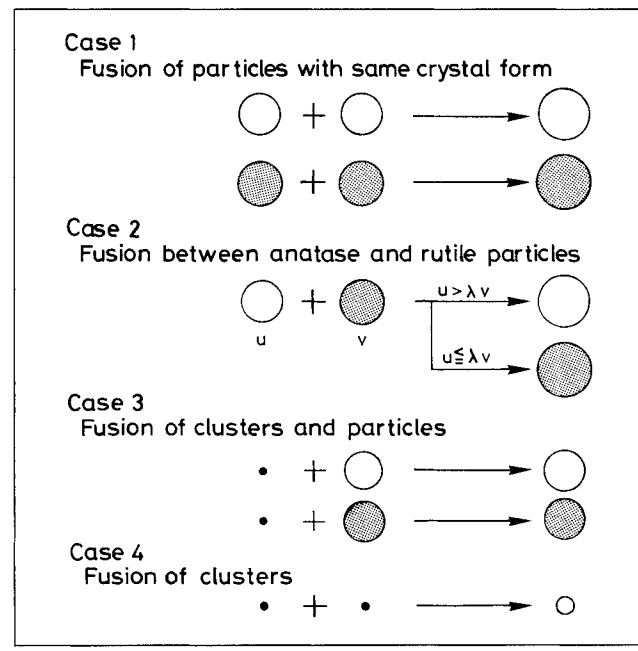

Figure 11. Transformation at coagulation.

White part, anatase; grey part, rutile

Table 3. Overall Probability for Transformation at $T \leqq 1{,}273$ K

Path No.	Probability for Formation of Rutile by Coagulation	Contributing Case(s)
①	$E_iE_j + {}^1W_{ij}(1-E_i)E_j + {}^1W_{ji}E_i(1-E_j)$	Cases 1 and 2
②	${}^1W_{\ell i}E_i(1-E_\ell) + E_\ell$	Cases 1 and 2
③	E_ℓ	Simple leaving
④	E_ℓ	Simple leaving
⑤	E_ℓ	Simple leaving
⑥	E_ℓ	Simple leaving
⑦	E_r	Case 4
⑧	0	Case 3
⑨	$2{}^1W_{\ell\ell}E_\ell(1-E_\ell) + E_\ell^2$	Cases 1 and 2

Case 3: Fusion between Cluster and Particle. The crystal phase of the particle is not changed by the fusion.

Case 4: Fusion of Clusters. The coagulation between clusters in the discrete region always produces an anatase cluster.

Table 3 summarizes the rutile mass fraction in the particle newly produced by each fusion path. E_ℓ is the rutile fraction in particles of size ℓ. For instance, the overall probability for path ① is composed of the contributions from cases 1 and 2 discussed above.

Multiplying each term in Eqs. 18 and 19 by the overall probability of rutile formation given in Table 3, the rutile mass in section ℓ, S_ℓ, is obtained as follows:

$1 \leqq \ell \leqq M'$:

$$\frac{dS_\ell}{dt} = \underbrace{\frac{1}{2}\sum_{i=1}^{\ell-1}\sum_{j=1}^{\ell-1} {}^1\bar{\beta}_{ij\ell}Q_iQ_j[E_iE_j + {}^1W_{ij}(1-E_i)E_j + {}^1W_{ji}E_i(1-E_j)]}_{①}$$

$$+ \underbrace{\sum_{i=1}^{\ell-1} {}^5\bar{\beta}_{i\ell}Q_iQ_\ell[{}^1W_{\ell i}E_i(1-E_\ell) + E_\ell]}_{②} - \underbrace{\sum_{i=1}^{\ell-1} {}^6\bar{\beta}_{i\ell}E_\ell Q_iQ_\ell}_{③}$$

$$\underbrace{-\frac{1}{2}{}^3\bar{\beta}_{\ell\ell}E_\ell Q_\ell^2}_{④} + \underbrace{\frac{1}{2}{}^7\bar{\beta}_{\ell\ell}Q_\ell^2[2{}^1W_{\ell\ell}E_\ell(1-E_\ell) + E_\ell^2]}_{⑨} - \underbrace{\sum_{i=\ell+1}^{M} {}^4\bar{\beta}_{i\ell}E_\ell Q_iQ_\ell}_{⑤}$$

$$\underbrace{-\sum_{i=1}^{9} {}^2\bar{\bar{\beta}}_{i\ell}E_\ell N_iQ_\ell}_{⑥} + \underbrace{\sum_{i=1}^{9}\sum_{r=1}^{\ell-1} {}^3\bar{\bar{\beta}}_{ir\ell}E_rN_iQ_r}_{⑦} + R_\ell \qquad (25)$$

$\ell > M'$:

$$\frac{dS_\ell}{dt} = \underbrace{\frac{1}{2}\sum_{i=1}^{M'}\sum_{j=1}^{M'} {}^1\bar{\beta}_{ij\ell}Q_iQ_j[E_iE_j + {}^1W_{ij}(1-E_i)E_j + {}^1W_{ji}E_i(1-E_j)]}_{①}$$

① (for coagulation of particles $i \leqq M'$ and $j \leqq M'$)

$$+ \underbrace{\sum_{i=1}^{M'}\sum_{j=M'+1}^{\ell-1} {}^1\bar{\beta}_{ij\ell}Q_iQ_j[(E_iE_j + {}^1W_{ij}(1-E_i)E_j + W_{ji}E_i(1-E_j)]}_{①}$$

① (for coagulation of particles $i \leqq M'$ and $j > M'$)

$$+ \underbrace{\sum_{i=1}^{M'} {}^5\bar{\beta}_{i\ell}Q_iQ_\ell[({}^1W_{\ell i}E_i(1-E_\ell) + E_\ell]}_{②} - \underbrace{\sum_{i=1}^{M'} {}^6\bar{\beta}_{i\ell}E_\ell Q_iQ_\ell}_{③}$$

$$\underbrace{-\sum_{i=1}^{9} {}^2\bar{\bar{\beta}}_{i\ell}E_\ell N_iQ_\ell}_{⑥} + \underbrace{\sum_{i=1}^{9}\sum_{r=1}^{\ell-1} {}^3\bar{\bar{\beta}}_{ir\ell}E_rN_iQ_r}_{⑦} + R_\ell \qquad (26)$$

Path ⑨ is the coagulation between particles which are both in section ℓ, the coagulated particle remaining in section ℓ. The coagulation coefficient for this path ⑨, not given by Wu and Flagan (1988), is expressed as follows:

$${}^7\bar{\beta}_{\ell\ell} = \int_{x_{\ell-1}}^{x_\ell}\int_{x_{\ell-1}}^{x_\ell} \frac{2\theta[(u+v) < v_\ell]\beta(u,v)}{v(x_\ell - x_{\ell-1})^2}\,dx\,dx \qquad (27)$$

Because the transformation from anatase to rutile below 1,273 K is controlled by surface nucleation, the transformation rate is proportional to the surface area of the particles. Then the spontaneous transformation rate for section ℓ is obtained by rearranging Eq. 9.

$$R_\ell = Q_\ell\frac{d\alpha_{R\ell}}{dt} = Q_\ell(6k_N/d_\ell)(1-\alpha_{R\ell}) \qquad (28)$$

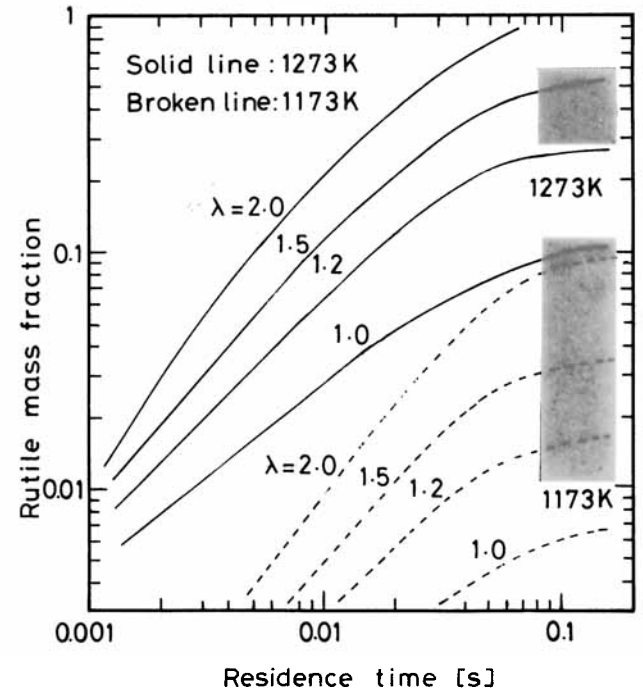

Figure 12. Rutile mass fraction produced at 1,173 K and 1,273 K.

where d_ℓ is the average size of particles in section ℓ. The relationship between $\alpha_{R\ell}$ and t is given by Eq. 11. The average fraction of the rutile phase in all the particles is calculated as:

$$M_R/(M_R+M_A)=\sum_{\ell=1}^{M} S_\ell \Big/ \sum_{\ell=1}^{M} Q_\ell \tag{29}$$

where the mass of clusters is neglected.

Figure 12 indicates the average rutile fraction produced at 1,173 K and 1,273 K. The solid lines show the results for 1,273 K and the broken lines those for 1,173 K. The experimental data of the rutile fraction, plotted in Figure 4, are indicated by the shadowed zones. If λ is taken in the range of 1.2–1.5, the prediction agrees well with the experimental values. When a rutile particle coagulates with an anatase particle 1.2–1.5 times heavier than itself, the new particle becomes rutile. This seems sound in view of the thermochemical stability of the rutile phase.

Formation at 1,373 K

At this temperature, the linear growth rate of the rutile phase toward the interior of the anatase particle is very slow in comparison with the transformation at 1,173 K. Particles belonging to the size section ℓ actually show a spectrum of rutile content. This spectrum is expressed by the rutile fraction coordinate w. The particle radius is divided into 25 subsections with an equal shell volume, 1/25, and the subsections are numbered by the suffix q. The surface and center of the particle are indicated by $q=0$ and 25 as shown in Figure 13. Particles whose rutile fraction is in the range of $w_q \sim w_{q-1}$ are designated to the rutile-fraction section q. Then the average rutile mass in the particles belonging to the size section ℓ and the rutile-fraction section q is expressed as:

$$\epsilon_{\ell q}=\frac{w_q+w_{q-1}}{2}\,\frac{x_\ell-x_{\ell-1}}{\exp(-x_{\ell-1})-\exp(-x_\ell)} \tag{30}$$

where the first factor on the right hand side is the average rutile fraction in the rutile fraction section q, the second factor the logarithmic average mass of a particle in the size section ℓ. The average anatase mass in the particles is obtained similarly.

$$\delta_{\ell q}=\left[1-\frac{w_q+w_{q-1}}{2}\right]\frac{x_\ell-x_{\ell-1}}{\exp(-x_{\ell-1})-\exp(-x_\ell)} \tag{31}$$

Figure 14 shows the cases that determine the rutile fraction after collision and fusion between particles belonging to size section h and rutile fraction section j and belonging to size section i and rutile fraction section k.

Case 1′: Fusion between Equal-Sized Particles ($h=i$). As fusion accompanies the reconstruction of TiO_2 crystal, a part of the anatase phase may be transformed to rutile in the course of fusion. If the rutile mass is much smaller than the anatase mass, however, the rutile phase will be incorporated into the anatase. Thus, the probability that the rutile fraction in the new particle belonging to section ℓ falls in the rutile fraction section q, ${}^2W_{hijk\ell q}$, depends on the rutile fraction in the initial particles.

a. The sum of anatase mass in initial particles is larger than λ times the sum of the rutile mass in the particles: $\delta_{hj}+\delta_{ik}>\lambda(\epsilon_{hj}+\epsilon_{ik})$. It is assumed that the fusion does not generate the rutile phase. Then, the newborn particle contains the rutile mass of $\epsilon_{hj}+\epsilon_{ik}$, which is presumed to exist in the peripheral region. The probability ${}^2W_{hijk\ell q}$ is given by

$${}^2W_{hijk\ell q}=\frac{\int_{x_{h-1}}^{x_h}\int_{x_{i-1}}^{x_i}\int_{w_{j-1}}^{w_j}\int_{w_{k-1}}^{w_k}\theta\left(e_{q-1}<\dfrac{uy+vz}{u+v}\leqq e_q\right)(u+v)\,dw\,dw\,dx\,dx}{(w_j-w_{j-1})(w_k-w_{k-1})\int_{x_{h-1}}^{x_h}\int_{x_{i-1}}^{x_i}(u+v)\,dx\,dx} \tag{32}$$

b. $\delta_{hj}+\delta_{ik}\leqq\lambda(\epsilon_{hj}+\epsilon_{ik})$. The initial particles are completely transformed to the rutile phase in the course of fusion. Then the new particle becomes pure rutile, and ${}^2W_{hijk\ell q}=0$ for $q=0$–24: ${}^2W_{hijk\ell q}=1$ for $q=25$.

Case 2′: Fusion between Particles Belonging to the Sections of Different Sizes ($h>i$). The definition of probability is the same as in Case 1′.

c. The anatase mass of the smaller particle is larger than λ times the sum of the rutile mass in the initial particles: $\delta_{ik}>\lambda(\epsilon_{hj}+\epsilon_{ik})$. The fusion does not generate the rutile phase, and the newborn particle contains a rutile mass of $\epsilon_{hj}+\epsilon_{ik}$. ${}^2W_{hijk\ell q}$ is given by Eq. 32.

d. $\delta_{ik}\leqq\lambda(\epsilon_{hj}+\epsilon_{ik})$. The total mass of the smaller particle is transformed to the rutile phase during the fusion, but the merger of the smaller particle cannot affect the structure of the larger particle. Then, the smaller particle is incorporated into the peripheral rutile zone of the larger particle. ${}^2W_{hijk\ell q}$ is given as follows:

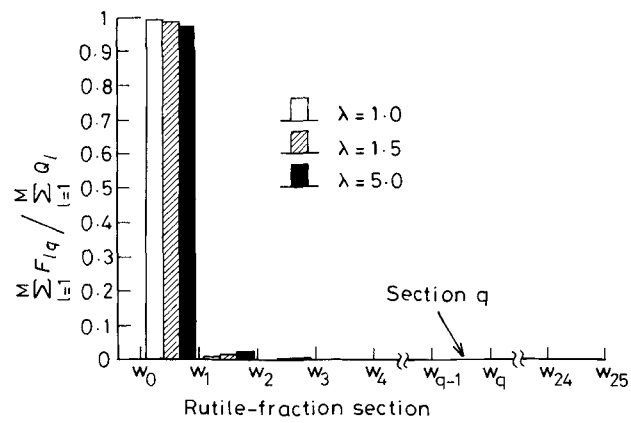

Figure 13. Distribution of rutile fraction in particles produced at 1,373 K.

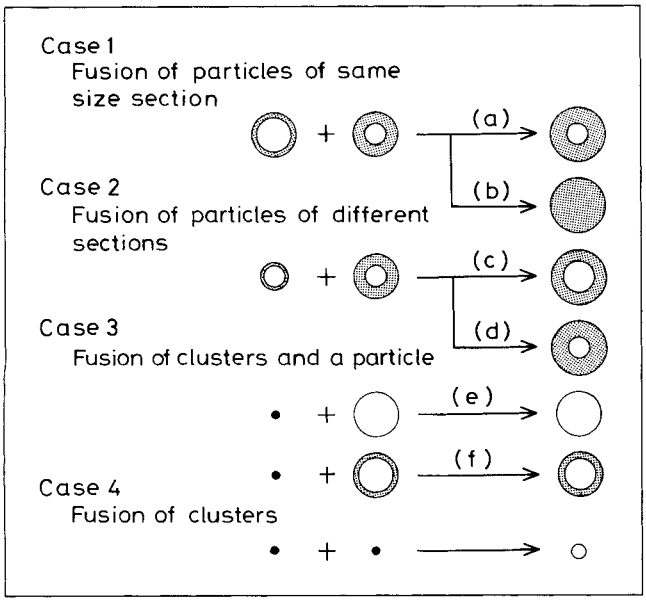

Figure 14. Cases determining rutile fraction after coagulation of two particles.

White part, anatase; grey part, rutile

$$ {}^{2}W_{hijk\ell q} = \frac{\int_{x_{h-1}}^{x_h}\int_{x_{i-1}}^{x_i}\int_{w_{k-1}}^{w_k}\theta\left(e_{q-1}<\frac{uy+v}{u+v}\leqq e_q\right)(u+v)\,dw\,dx\,dx}{(w_k-w_{k-1})\int_{x_{h-1}}^{x_h}\int_{x_{i-1}}^{x_i}(u+v)\,dx\,dx} \tag{33} $$

Case 3': Fusion between a h-mer Cluster in the Discrete Regime and a Particle of the Size Section i. The probability that the rutile mass fraction in the new particle of the size ℓ falls in the rutile fraction section q is denoted by ${}^{3}W_{hij\ell q}$.

e. Fusion with an anatase particle ($j=0$). The crystal form of new particles is anatase. Thus, ${}^{3}W_{hij\ell q}=1$ for $q=0$; ${}^{3}W_{hij\ell q}=0$ for $q=1$–25.

f. Fusion with a particle of the rutile fraction section j. The cluster is incorporated into the rutile phase existing on the surface of the particle, and the rutile phase is grown by the deposition of the h-mer cluster whose mass is hm_c. ${}^{3}W_{hij\ell q}$ is given by

$$ {}^{3}W_{hij\ell q} = \frac{\int_{x_{i-1}}^{x_i}\int_{w_{j-1}}^{w_j}\theta\left(e_{q-1}<\frac{hm_c+yu}{hm_c+u}\leqq e_q\right)(hm_c+u)\,dw\,dx}{(w_j-w_{j-1})\int_{x_{i-1}}^{x_i}(hm_c+u)\,dx} \tag{34} $$

Case 4': Fusion between Clusters. An anatase particle is generated if the mass of the new particle is larger than $9m_c$. If ${}^{4}W_{ij\ell q}$ is defined as the probability that the rutile mass fraction in the new particle of size ℓ falls in the rutile fraction section q, then ${}^{4}W_{ij\ell q}=1$ for $q=0$ and ${}^{4}W_{ij\ell q}=0$ for $q=1$–25.

$F_{\ell q}$, the mass of particles in the size section ℓ and the rutile fraction section q, is obtained in the same manner as in Eqs. 25 and 26.

$\underline{1\leqq\ell\leqq M'}$:

$$ \frac{dF_{\ell q}}{dt} = \underbrace{\frac{1}{2}\sum_{i=1}^{\ell-1}\sum_{j=1}^{\ell-1}\sum_{k=0}^{25}\sum_{h=0}^{25}{}^{1}\bar{\beta}_{ij\ell}{}^{2}W_{ijkh\ell q}F_{ik}F_{jh}}_{①} $$

$$ + \underbrace{\sum_{i=1}^{\ell-1}\sum_{k=0}^{25}\sum_{h=0}^{25}{}^{5}\bar{\beta}_{i\ell}{}^{2}W_{i\ell kh\ell q}F_{ik}F_{\ell h}}_{②} - \underbrace{\sum_{i=1}^{\ell-1}\sum_{k=0}^{25}{}^{6}\bar{\beta}_{i\ell}F_{ik}F_{\ell q}}_{③} $$

$$ \underbrace{-\frac{1}{2}\sum_{h=0}^{25}{}^{3}\bar{\beta}_{\ell\ell}F_{\ell h}F_{\ell q}}_{④} + \underbrace{\frac{1}{2}\sum_{k=0}^{25}\sum_{h=0}^{25}{}^{7}\bar{\beta}_{\ell\ell}{}^{2}W_{\ell\ell kh\ell q}F_{\ell h}F_{\ell k}}_{⑨} $$

$$ \underbrace{-\sum_{i=\ell+1}^{M}{}^{4}\bar{\beta}_{i\ell}F_{\ell q}Q_i}_{⑤} \underbrace{-\sum_{i=1}^{9}{}^{2}\bar{\bar{\beta}}_{i\ell}N_iF_{\ell q}}_{⑥} $$

$$ \underbrace{+\sum_{i=1}^{9}\sum_{r=1}^{\ell-1}\sum_{k=0}^{25}{}^{3}\bar{\bar{\beta}}_{ir\ell}{}^{3}W_{irk\ell q}F_{rk}N_i}_{⑦} + \underbrace{\frac{1}{2}\sum_{i=1}^{9}\sum_{j=1}^{9}{}^{4}\bar{\bar{\beta}}_{ij}{}^{4}W_{i\ \ell q}N_iN_j}_{⑧} $$

$$ + R_{\ell q} \tag{35} $$

$\underline{\ell>M'}$:

$$ \frac{dF_{\ell q}}{dt} = \underbrace{\frac{1}{2}\sum_{i=1}^{M'}\sum_{j=1}^{M'}\sum_{k=0}^{25}\sum_{h=0}^{25}{}^{1}\bar{\beta}_{ij\ell}{}^{2}W_{ijkh\ell q}F_{ik}F_{jh}}_{① \text{ (for coagulation of particles } i\leqq M' \text{ and } j\leqq M')} $$

$$ + \underbrace{\sum_{i=1}^{M'}\sum_{j=M'+1}^{\ell-1}\sum_{k=0}^{25}\sum_{h=0}^{25}{}^{1}\bar{\beta}_{ij\ell}{}^{2}W_{ijkh\ell q}F_{ik}F_{jh}}_{① \text{ (for coagulation of particles } i\leqq M' \text{ and } j>M')} $$

$$ + \underbrace{\sum_{i=1}^{M'}\sum_{k=0}^{25}\sum_{h=0}^{25}{}^{5}\bar{\beta}_{i\ell}{}^{2}W_{i\ell kh\ell q}F_{ik}F_{\ell h}}_{②} - \underbrace{\sum_{i=1}^{M'}\sum_{k=0}^{25}{}^{6}\bar{\beta}_{i\ell}F_{ik}F_{\ell q}}_{③} $$

$$ \underbrace{-\sum_{i=0}^{9}{}^{2}\bar{\bar{\beta}}_{i\ell}N_iF_{\ell q}}_{⑥} + \underbrace{\sum_{i=1}^{9}\sum_{r=1}^{M'}\sum_{k=0}^{25}{}^{3}\bar{\bar{\beta}}_{ir\ell}{}^{3}W_{irk\ell q}F_{rk}N_i}_{⑦} $$

$$ + \underbrace{\frac{1}{2}\sum_{i=1}^{9}\sum_{j=1}^{9}{}^{4}\bar{\bar{\beta}}_{ij}{}^{4}W_{ij\ell q}N_iN_j}_{⑧} + R_{\ell q} \tag{36} $$

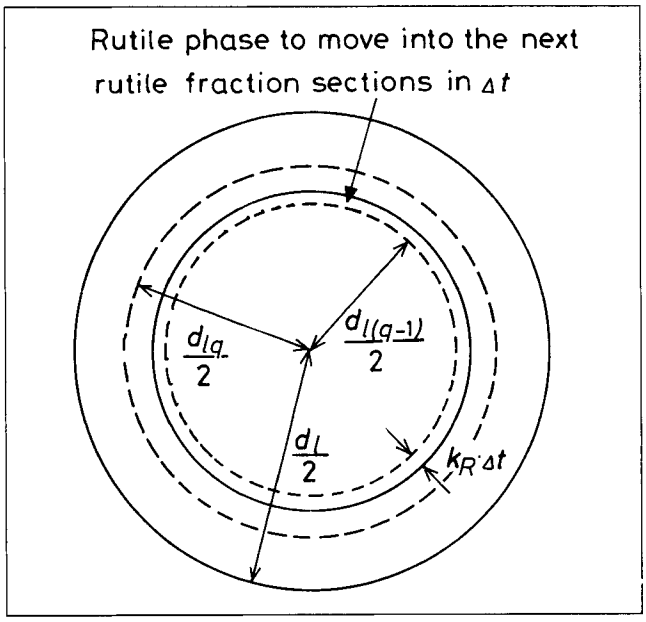

Figure 15. Moving rutile front.

$R_{\ell q}$ in Eqs. 35 and 36 is the rate of the rutile mass entering the rutile fraction section q by spontaneous transformation. The number of pure anatase particles ($q=0$) is decreased by the formation of rutile nucleus on the surface. Then, $R_{\ell q}$ for $q=0$ (i.e., $R_{\ell 0}$), which is always negative, can be obtained from Eq. 28.

$$R_{\ell 0} = -Q_\ell \left.\frac{d\alpha_{R\ell}}{dt}\right|_{q=0} = -(6k_N/d_\ell)F_{\ell 0} \tag{37}$$

where $F_{\ell 0}$ is the total mass of pure anatase particles in the size section ℓ and is given by

$$F_{\ell 0} = (1-\alpha_{R\ell})Q_\ell \tag{38}$$

Figure 15 shows a schematic model of the moving rutile front in a particle of the size section ℓ. If the rutile fraction in this particle is w_q, the diameter of the anatase core is:

$$d_{\ell q} = d_\ell (1-w_q)^{1/3} \tag{39}$$

Assume that the rutile front is now located in section q bounded by $d_{\ell q}$ and $d_{\ell(q-1)}$. After a short time Δt, the rutile phase advances by $k_R \Delta t$, and a part of the rutile phase leaves the rutile fraction section q.

$$\frac{\text{Mass leaving section } q \text{ in } \Delta t}{\text{Mass in section } q} = \frac{(d_{\ell q}+2k_R\Delta t)^3 - d_{\ell q}^3}{d_{\ell(q-1)}^3 - d_{\ell q}^3} \doteqdot \frac{6d_{\ell q}^2 k_R \Delta t}{d_{\ell(q-1)}^3 - d_{\ell q}^3} \tag{40}$$

The last term was obtained by the Taylor expansion of the numerator in the second term for $d_{\ell q} >> 2k_R\Delta t$. Then, the rate of the rutile mass entering the rutile fraction section 1 (i.e., $R_{\ell 1}$), which is negative or positive, is obtained by modifying $R_{\ell 0}$.

$$R_{\ell 1} = -R_{\ell 0} - \frac{6d_{\ell 1}^2 k_R}{d_{\ell 0}^3 - d_{\ell 1}^3} F_{\ell 1} \tag{41}$$

The term prefixed to $F_{\ell 1}$ is the normalized mass of particles leaving the rutile fraction section 1 per time period Δt. In the range of $i=2$–24, $R_{\ell q}$ is given by

$$R_{\ell q} = \frac{6d_{\ell(q-1)}^2 k_R}{d_{\ell(q-2)}^3 - d_{\ell(q-1)}^3} F_{\ell(q-1)} - \frac{6d_{\ell q}^2 k_R}{d_{\ell(q-1)}^3 - d_{\ell q}^3} F_{\ell q} \tag{42}$$

$R_{\ell q}$ for $q=25$, $R_{\ell 25}$, is zero because the rutile phase reaches the center of the particle. Therefore, the average mass fraction of the rutile phase in all particles is obtained by

$$M_R/(M_A+M_R) = \sum_{\ell=1}^{M}\sum_{q=1}^{25} \frac{w_q + w_{q-1}}{2} F_{\ell q} \Big/ \sum_{\ell=1}^{M} Q_\ell \tag{43}$$

The computation was carried out using the values of k_N and k_R for 1,373 K given by Eq. 15, and the result is shown in Figure 13. The parameter λ was changed in the range of 1.0–5.0. Even if λ was increased to 5.0, most of the particles are in the first section of the rutile mass fraction distribution. As shown in Figure 4, the rutile mass fraction of TiO_2 produced by the reaction between $TiCl_4$ and O_2 at 1,373–1,473 K was very low. This experimental result is explained well by the above simulation.

Conclusion

TiO_2 fine particles were produced by the gas-phase reaction of $TiCl_4$ with O_2 in aerosol reactors, and the effect of reaction conditions on the particle size and the rutile content were investigated.

TiO_2 particles smaller than 15 nm could be sintered at 1,273 K in 0.16 s. The particle sizes obtained experimentally, however, were 55–65 nm. This means that the growth of particles proceeded through the deposition of monomer or small particles generated in the latter stage of reaction. The defect concentration in the TiO_2 particles strongly affected the transformation rate from anatase to rutile. The mass fraction of rutile increased with increasing reaction temperature in the range of $T \leqq 1{,}273$ K and with decreasing temperature above 1,273 K. Based on the experimental results, the whole process of TiO_2 particles generation was simulated by a population model developed in this article. This model can be applied to other processes by changing the values of parameters such as k_{TO}, bD_b, k_N, and k_R.

Acknowledgment

We are grateful to Professors Akio Kato and Junichi Hojo of the Dept. of Applied Chemistry, Kyushu Univ., for their valuable discussions. We also thank Professor Yoshitsugu Tomokiyo, Research Lab. of High Voltage Electron Microscope, Kyushu Univ.

Notation

bD_b = grain boundary diffusivity, $m^3 \cdot s^{-1}$
D_{O_2} = diffusivity of O_2, $m^2 \cdot s^{-1}$
d_ℓ = particle size of section ℓ, m
$d_{\ell q}$ = diameter of anatase core, m
d_n = inner diameter of nozzle, m

d_t = inner diameter of reactor, m
E_ℓ = rutile mass fraction in particles for size section ℓ
e_q = rutile mass fraction in particles belonging to rutile fraction section q, used in integral
$F_{\ell q}$ = mass concentration in size section ℓ and rutile fraction section q at 1,373 K, $kg \cdot m^{-3}$
$f_R(t)$ = volume fraction of rutile in particles at time t
I_A = X-ray diffraction intensity corresponding to anatase
I_R = X-ray diffraction intensity corresponding to rutile
$J_0(x)$ = Bessel function of first kind of zero-order
$J_1(x)$ = Bessel function of first kind of first-order
K_c = proportional coefficient for quantitative analysis of anatase-rutile mixture with X-ray diffraction
k_B = Boltzmann constant, $J \cdot K^{-1}$
k_N = evolution rate constant of rutile nucleus, $m \cdot s^{-1}$
k_R = linear growth rate of rutile phase, $m \cdot s^{-1}$
k_{TO} = reaction rate constant, s^{-1}
L = length of reactor, m
ℓ_n = neck length, m
M = largest section number corresponding to largest particle
M' = section number of sinterable limit
M_A = anatase mass in the mixture, kg
M_R = rutile mass in the mixture, kg
m_c = mass of monomer, kg
N_i = number concentration of i-mer, m^{-3}
p_{O_2} = partial pressure of O_2, Pa
p_{TiCl_4} = partial pressure of $TiCl_4$, Pa
$Q_a(A)$ = volumetric flow rate in annular space of A component measured at 298 K, $m^3 \cdot s^{-1}$
$Q_n(A)$ = volumetric flow rate in nozzle space of A component measured at 298 K, $m^3 \cdot s^{-1}$
Q_s = volumetric flow rate in sheath space measured at 298 K, $m^3 \cdot s^{-1}$
Q_ℓ = mass concentration of section ℓ, $kg \cdot m^{-3}$
R = gas constant, $J \cdot mol^{-1} \cdot K^{-1}$
R_ℓ = transformation rate for section ℓ below 1,273 K, $kg \cdot m^{-3} \cdot s^{-1}$
$R_{\ell q}$ = spontaneous transformation rate at 1,373 K, $kg \cdot m^{-3} \cdot s^{-1}$
r = radial coordinate used in Eq. A1, m
r_I = sphere radius, m
S_ℓ = rutile particles mass concentration for section ℓ at temperature below 1,273 K, $kg \cdot m^{-3}$
T = temperature, K
t = time, s
Δt = time difference, s
t_0 = annealing time, s
u,v = particle mass per increment Δx, used in integral, kg
v_ℓ = mass of a particle in size section ℓ, used in integral, kg
w_q = rutile fraction in rutile fraction section q
x_ℓ = logarithm of particle mass in size section ℓ
$Y_0(x)$ = Bessel function of second kind of zero-order
$Y_1(x)$ = Bessel function of second kind of first-order
y,z = rutile fraction per increment Δw in the particle mass u and v, respectively, used in integral

Greek letters

α_R = number-based fraction of rutile covered particles for equal sized system
$\alpha_{R\ell}$ = number-based fraction of rutile covered particles in size section ℓ
α_{R0} = α_R at $t = 0$
$\beta(u,v)$ = Brownian coagulation rate function between particles of mass u and v, used in integral, $m^{-3} \cdot s^{-1}$
β_{ij} = $\beta(u,v)$ for $u:x_i$ and $v:x_j$, $m^{-3} \cdot s^{-1}$
γ = surface tension, $J \cdot m^{-2}$
$\delta_{\ell q}$ = average anatase mass in particles belonging to size section ℓ and rutile fraction section q, kg
$\epsilon_{\ell q}$ = average rutile mass in particles belonging to size section ℓ and rutile fraction section q, kg
ζ = variable used in integral
θ = unit function
λ = parameter
ξ = dimensionless radius of nozzle jet, $2r/d_n$
τ = dimensionless time, $4D_{O_2}t/d_n^2$
Ω = volume of oxygen ion, m^3

Literature Cited

Anderson, H. U., "Initial Sintering of Rutile," *J. Amer Ceram. Soc.*, **50**, 235 (1967).
Astier, M., and P. Vergnon, "Determination of the Diffusion Coefficient from Sintering Data of Ultrafine Oxide Particles," *J. Solid State Chem.*, **19**, 67 (1976).
Carslaw, H. S., and J. C. Jaeger, *Conduction of Heat in Solids*, 2nd ed., Oxford Univ. Press, p. 346 (1959).
Coblenz, W. S., J. M. Dynys, R. M. Cannon, and R. L. Coble, "Initial Stage Solid State Sintering Models: a Critical Analysis and Assessment," *Mat. Sci. Res.*, **13**, 141 (1980).
Fuchs, N. A., *The Mechanics of Aerosols*, Pergamon Press, Oxford (1964).
Gelbard, F., Y. Tambour, and J. H. Seinfeld, "Sectional Representations for Simulating Aerosol Dynamics," *J. Colloid and Interface Sci.*, **76**, 541 (1980).
George, A. P., R. D. Murley, and E. R. Place, "Formation of TiO_2 Aerosol from Combustion Supported Reaction of $TiCl_4$ and O_2," *Symp. Farad. Soc.*, **7**, 63 (1973).
Hirschfelder, J. O., C. F. Curtiss, and R. B. Bird, *Molecular Theory of Gases and Liquids*, Wiley, New York (1964).
Kato, A., and Y. Suyama, "Preparation of Rutile Powders by Vapor Phase Reaction of $TiCl_4$-H_2-CO_2 System," *Chem. Lett.*, 961 (1974).
Levenspiel, O., *Chemical Reaction Engineering*, 2nd ed., Wiley, New York, p. 357 (1972).
Mackenzie, K. J. D., "The Calcination of Titania: V Kinetics and Mechanism of the Anatase-Rutile Transformation in the Presence of Additives," *Trans. J. Brit. Ceram. Soc.*, **74**, 77 (1975).
Matsumoto, A., N. Sakamoto, J. Shiokawa, H. Tamura, and T. Ishino, "Production of TiO_2 of Rutile by Gas Phase Oxidation of $TiCl_4$," *Kogyo Kagaku Zasshi*, **70**, 2115 (1967).
Morooka, S., T. Yasutake, A. Kobata, K. Ikemizu, and Y. Kato, "A Mechanism for the Production of Ultrafine Particles of TiO_2 by a Gas Phase Reaction," *Int. Chem. Eng.*, **29**, 119 (1989).
Nichols, F. A., and W. W. Mullins, "Morphological Changes of a Surface of Revolution due to Capillarity-Induced Surface Diffusion," *J. Appl. Phys.*, **36**, 1826 (1965).
Okuyama, K., Y. Kousaka, N. Tohge, S. Yamamoto, J. J. Wu, R. C. Flagan, and J. H. Seinfeld, "Production of Ultrafine Metal Oxide Aerosol Particles by Thermal Decomposition of Metal Alkoxide Vapors," *AIChE J.*, **32**, 2010 (1986).
Spurr, A., and H. Myers, "Quantitative Analysis of Anatase-Rutile Mixtures with an X-Ray Diffractometer," *Anal. Chem.*, **29**, 760 (1957).
Suyama, Y., K. Ito, and A. Kato, "Mechanism of Rutile Formation in Vapor Phase Oxidation of $TiCl_4$ by Oxygen," *J. Inorg. Nucl. Chem.*, **37**, 1883 (1975).
Suyama, Y., and A. Kato, "TiO_2 Produced by Vapor-Phase Oxygenolysis of $TiCl_4$," *J. Amer. Ceram. Soc.*, **59**, 146 (1976).
Toyama, S., M. Nakamura, H. Mori, T. Nachi, and K. Kanai, "Production of Ultrafine Particles by Gas Phase Oxidation of Chlorides," Meeting of Soc. Chem. Engrs., Japan, p. 322 (1990).
Ulrich, G. D., "Theory of Particle Formation and Growth in Oxide Synthesis Flame," *Combust. Sci. Technol.*, **4**, 47 (1971).
Ulrich, G. D., and J. W. Riehl, "Aggregation and Growth of Submicron Oxide Particles in Flames," *J. Colloid and Interface Sci.*, **87**, 257 (1982).
Wu, J. J., and R. C. Flagan, "A Discrete-Sectional Solution to the Aerosol Dynamic Equation," *J. Colloid and Interface Sci.*, **123**, 339 (1988).

Appendix

The diffusion rate of oxygen through the cylindrical boundary is described by

$$\frac{\partial p_{O_2}}{\partial t} = \frac{1}{r}\frac{\partial}{\partial r}\left(rD_{O_2}\frac{\partial p_{O_2}}{\partial r}\right) \tag{A1}$$

The initial and boundary conditions are

$$t=0;\ r\geqq d_n/2,\ p_{O_2}=p_{O_{20}};\ r<d_n/2,\ p_{O_2}=0$$
$$t>0;\ r=0,\ p_{O_2}=\text{finite};\ r=\infty,\ p_{O_2}=p_{O_{20}} \tag{A2}$$

where $d_n/2$ is the radius of the nozzle jet. The dimensionless analytical solution for the inside of the cylindrical zone is given by Carslaw and Jaeger (1959).

$$\frac{p_{O_2}(\xi,\tau)}{p_{O_{20}}}=1-\frac{4}{\pi^2}\int_0^\infty \frac{\exp(-\tau\zeta^2)J_0(\zeta\xi)J_1(\zeta)}{\zeta^2[J_1(\zeta)Y_0(\zeta)-J_0(\zeta)Y_1(\zeta)]^2}\,d\zeta \tag{A3}$$

The value of D_{O_2} is estimated from the correlation of Hirschfelder et al. (1964). The calculation using the present experimental conditions indicates that the oxygen concentration exceeds the initial $TiCl_4$ concentration within 10 ms. The nozzle gas travels only 3–7 mm from the mouth in this period. This distance is equivalent to the nozzle diameter and is less than 5% of the heated zone length. It was found experimentally that the reaction rate was independent of the oxygen concentration. Mixing between O_2 and $TiCl_4$ was thus attained very quickly compared with the residence time in the reaction zone.

Manuscript received Aug. 13, 1990, and revision received Dec. 11, 1990.